Kinetics of Carbon Monoxide Migration and Binding in Solvated Myoglobin as Revealed by Molecular Dynamics Simulations and Quantum Mechanical Calculations

Marco D'Abramo,[†,‡] Alfredo Di Nola,[§] and Andrea Amadei*[,⊥]

Institut de Recerca Biomèdica, Parc Cientific de Barcelona Josep Samitier 1-5, Barcelona 08028 and Barcelona Supercomputing Center Jordi Girona 29, Barcelona 08034, Spain, Departament de Bioquimica, Facultat de Biologia, Universitat de Barcelona, Avgda Diagonal 647 Barcelona 08028, Spain, Dipartimento di Chimica, Università di Roma "La Sapienza", P.le A. Moro 5 00185 Rome, Italy, and Departimento di Scienze e Tecnologie Chimiche, Università di Roma "Tor Vergata", via della Ricerca Scientifica 00133 Rome, Italy

Received: April 6, 2009; Revised Manuscript Received: October 26, 2009

By using multiple (independent) molecular dynamics (MD) trajectories (about 500 ns in total) of photolized carbon monoxide (CO) within solvated myoglobin, a quantitative description of CO migration and corresponding kinetics is obtained. MD results combined with previously reported quantum mechanical calculations on the CO−heme binding−unbinding reaction step in myoglobin allowed construction of a detailed quantitative model, shedding light on the kinetic mechanism and relevant steps of CO migration and geminate binding. Finally, the obtained (unbiased) theoretical−computational model is critically compared with the available computational and experimental data for myoglobin in solution.

Introduction

Myoglobin (Mb) is probably one of the most studied proteins, which long served as a model system for investigating ligand binding, migration, and conformational relaxation in proteins.[1–19] Many of these investigations exploit the light sensitivity of the Mb complex with carbon monoxide (CO). The exposure of the Myoglobin carbon monoxide adduct to a monochromatic light pulse breaks the iron−CO bond, initiating a series of spectroscopic and structural changes which may be monitored using different experimental techniques. In the last years, several quantitative analyses concerning the structural dynamics of Mb and ligand diffusion, with picosecond to millisecond time resolution, have been obtained by time-resolved Laue diffraction experiments. Since the pioneering work on wild-type sperm whale Mb (wt-Mb) carried out at room temperature,[4,5] molecular movies have been produced with high spatial resolution and wide temporal sampling on a series of Mb mutants at various experimental conditions.[6–10] Such studies provided a large body of data showing that CO migration in crystallized Mb is determined by a set of transition steps between Mb cavities,[2,3] associated with nanoseconds time range relaxations.[4,5]

Characterization of ligand migration in solvated Mb is much more complex due to the lack of direct evaluation of the time-dependent CO occupancies of Mb cavities. In the last decades a huge number of experimental studies, essentially based on CO geminate binding reaction data, have been devoted to unveiling the kinetic mechanism of ligand migration and binding in solvated Mb. However, the difficulties of characterizing the whole process due to the inherent complexity of the geminate binding reaction given by the superposition of binding and migration steps allowed the proliferation of different, often contradictory, models. In particular, the kinetic role and significance of Mb conformational relaxation in the binding and migration reaction steps at physiological conditions (room temperature) is still rather controversial. In fact, at low temperature (below 270 K), geminate binding reaction data provide a clear nonexponential relaxation, phenomenologically described by the stretched exponential decay and physically interpreted in terms of multiple reaction paths and kinetic coupling between CO migration/binding and Mb conformational relaxation processes.[15,16] At room temperature, on the contrary, experimental data may be also accurately described by simple exponential decays, possibly suggesting averaging of Mb conformations during the binding/migration kinetic steps. For room-temperature, wild-type Mb, the simple kinetic scheme proposed by Henry et al.,[14] providing a single exponential decay for CO escape and geminate binding and based on a pre-equilibrium of protein conformational fluctuations and CO distribution in Mb, is considered a proper description by many authors[14–16,18,20–22] but is in marked contrast with the conclusions of other authors[17,23] claiming that Mb relaxation occurs at a comparable or slower rate than binding/migration ones even at room temperature, leading to the use of models based on multiple kinetically distinguished Mb/CO reactive transitions.

Theoretical−computational studies, although they provided a large body of valuable information, did not yet allow for a conclusive picture of CO binding/migration in Mb. In fact, given the complexity of the process, theoretical−computational investigations on Mb/CO reaction events have either been focused on the CO−heme binding−unbinding reaction step only[24,25] via standard quantum chemical calculations with extremely simplified modeling of the protein−solvent effects or attempted to construct a kinetic model for binding/migration steps by using severe approximations[26,27] essentially based on simplified diffusion models for describing CO migration and (classical) empirical potential energy functions to treat the binding−unbinding reaction.

In a previous paper,[28] we reported a theoretical−computational study on the CO−heme binding−unbinding reaction in solvated

* To whom correspondence should be addressed. Tel.: 0039 06 72594905. Fax: 0039 06 72594328. E-mail: andrea.amadei@uniroma2.it.
[†] Institut de Recerca Biomèdica and Barcelona Supercomputing Center Jordi Girona.
[‡] Universitat de Barcelona.
[§] Università di Roma "La Sapienza".
[⊥] Università di Roma "Tor Vergata".

10.1021/jp903165p
Published on Web 11/24/2009

Mb, as obtained by using the perturbed matrix method[29–31] (PMM). Such a method, based on rigorous quantum mechanical calculations and explicitly treating at atomistic detail the perturbation due to the environment acting on the electronic states, allowed an accurate quantitative description of the electronic behavior in complex systems,[32] providing in the last years a proper modeling of UV/IR spectroscopy[31,33,34] and chemical reactions[29,35,36] in liquids and proteins. In our previous paper,[28] we obtained the free-energy profile along the reaction coordinate (the carbon−iron distance) in the range of CO−heme bond formation/disruption (0.18−0.38 nm), which served to obtain the corresponding reaction kinetics by solving a Fokker−Planck equation for the diffusion along the reaction free-energy surface. In a more recent publication on crystallized Mb,[37] we showed that the use of multiple MD trajectories may provide a quantitative description of CO migration kinetics, as obtained by atomistic simulations without any simplifying assumption, reproducing accurately the basic features of Mb/CO in the crystal state.

In the present paper, following our publication[37] on crystallized Mb, we use multiple MD simulations at 293 K (32 trajectories of 15 ns each) to construct a quantitative model for CO migration kinetics. Moreover, by using the reaction free-energy profile as provided by PMM,[28] together with the free-energy variation along the carbon−iron distance beyond 0.38 nm, as obtained by MD simulation data for the CO molecule within the distal pocket, we obtain the complete binding−unbinding reaction free-energy profile and, hence, utilizing the same theoretical approach described in our previous paper,[28] the corresponding binding−unbinding reaction kinetics. Finally, the combined use of binding−unbinding and migration kinetic steps as provided by the theoretical−computational procedure outlined furnishes a detailed quantitative kinetic model for the complete CO geminate binding and escape in solvated myoglobin at room temperature, to be compared to the available experimental data.

Methods

A total of 32 simulations (each of 15 ns) of solvated sperm whale myoglobin with photodissociated carbon monoxide were performed.

A structure extracted from a MD simulation of the covalently bound CO in solvated Mb at 293 K[28] with the protein hydrated with 6741 single point charge SPC water molecules[38] at liquid density (about 50 mol/L) was used for initial coordinates. Such a simulation box guaranteed that separation between the Mb/CO external atoms and box margin was never below 1.0 nm.

In order to simulate photodissociated CO in Mb, we replaced the CO−Fe bond with a nonbonded interaction, providing different initial velocities as obtained by the Maxwellian distribution at 293 K. In this way, the independent 32 MD trajectories provided a time-dependent CO distribution, mimicking the experimental relaxation kinetics induced by photolysis.

The simulations were performed with the Gromacs software package[39] using the GROMOS96 force field.[40] The CO molecules were modeled with the three-site "quadrupolar" CO model,[41] and according to previous theoretical and experimental results,[42–44] the His64(E7) side chain was modeled with hydrogen at the ε position. Note that more sophisticated CO models are nowadays available[45] involving fluctuating charges coupled to the intramolecular stretching coordinate. However, in this study, we employed the simpler three-site quadrupolar model, providing the essential features of carbon monoxide, in order to be coherent with our previous data[28,37] as obtained via the quadrupolar model and hence to properly compare our present results with the previous ones.

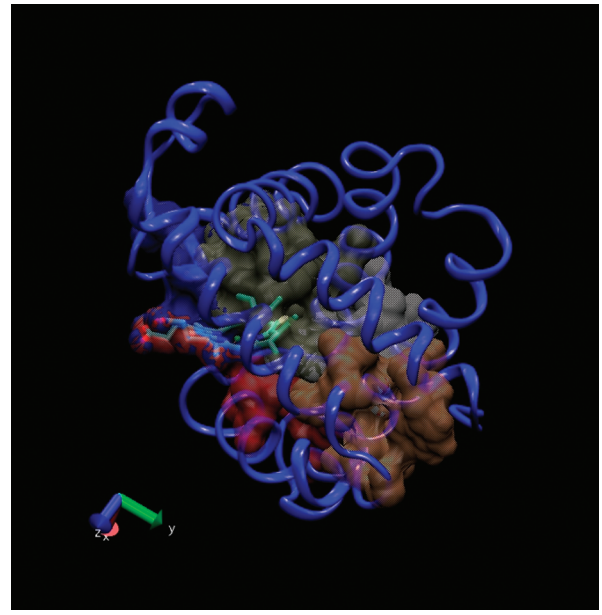

Figure 1. Schematic view of the Mb fold and location of the CO sites; DP blue, Xe1 red, Xe2 gray, Xe3 orange, and Xe4 green.

Statistical mechanically coherent canonical ensemble (NVT) conditions for the simulations were provided by the isothermal temperature coupling[46] and a constant volume box, using periodic boundary conditions. The bond lengths were constrained by using the LINCS algorithm.[47] A time step of 2 fs was used in all simulations. The Particle Mesh Ewald (PME) method[48] was used for the calculation of the long-range interactions with a grid spacing of 0.12 nm combined with a fourth-order B-spline interpolation to compute the potential and forces in between grid points. A nonbonded pair list cutoff of 9 Å was used for short-range interactions, and the pair list was updated every five time steps. During the simulations, each CO position was assigned to a specific CO site (i.e., distal pocket or one of the xenon cavities) by evaluating at each MD frame the residues forming the cavity around the ligand, hence defining one of the possible CO sites. When no actual cavity was found around the ligand, after visual inspection, CO was assigned to the free ligand state. Note that several ligand exchanges between sites were present, ensuring a proper sampling of the transitions (see Supporting Information).

All of the details on the PMM theoretical framework and calculations as well as on the procedure employed to obtain the binding−unbinding kinetic rate constants can be found in our previous paper.[28] Note that the diffusion constant along the reaction coordinate employed to solve the Fokker−Planck equation for the binding−unbinding reaction process, estimated in our previous paper by means of several short MD simulations with unconstrained chemical bonds,[28] is rather high (about 0.0042 nm^2/ps), being close to usual free diffusion constants.[27,53]

Results

Migration Kinetics. During the MD simulations, CO migrated from the distal pocket to the Xe1 cavity (see Figure 1) following essentially the same pathway as that found in crystallized Mb,[5,13,37] which involves the Xe4 and Xe3 cavities and the other two minor cavities, called phantom1 (Ph1, connected to Xe4) and phantom2 (Ph2, connected to Xe3), detected in previous computational studies.[49,50] Following our previous paper on CO migration kinetics in Mb crystals,[37] we simplify the kinetic model to be used by considering Ph1 and

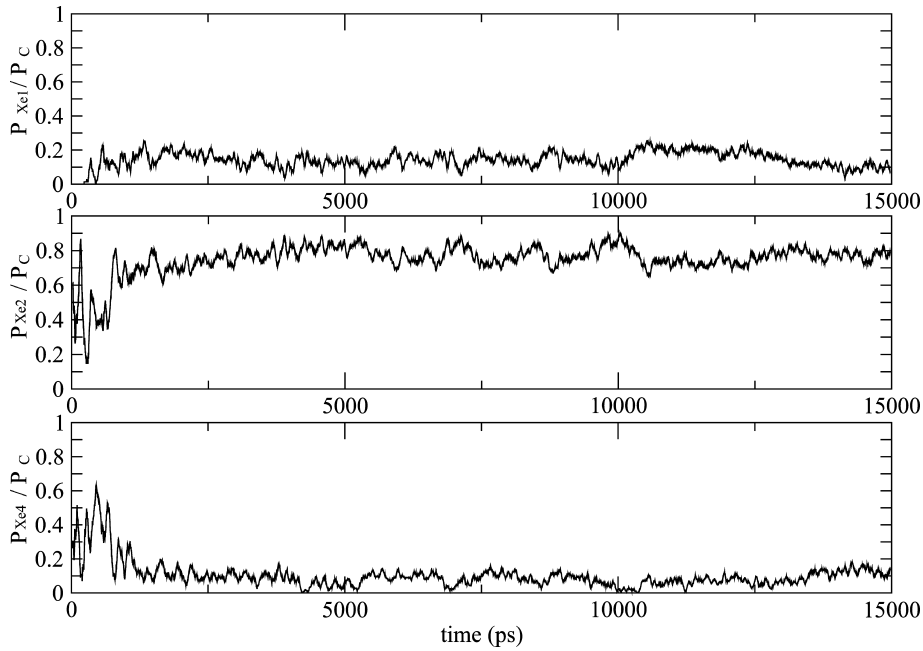

Figure 2. Time dependence of the xenon cavities' CO fractions relative to the site C overall probability, as obtained by MD data.

Ph2 as included in the Xe4 and Xe3 cavities, respectively, and, given the fact that the contiguous Xe1 and Xe2 proximal cavities are both accessed from Xe3, we also consider them as a single proximal site (Xe_p). Within such a definition of the CO sites, the general kinetic scheme (up to microseconds) for CO diffusion in Mb is

$$\text{Mb} + \text{CO} \leftarrow \text{DP} \rightleftarrows \text{Xe4} \rightleftarrows \text{Xe3} \rightleftarrows \text{Xe}_p$$

where DP is the distal pocket and Mb + CO denotes the free ligand state (typically, ligand escape may still be considered as virtually irreversible in the microseconds time range). Note that just as for the crystal case,[37] also for solvated Mb, our data indicate that the Xe3 cavity is the CO diffusion intermediate between Xe4 and Xe_p, in contrast with the model sometimes hypothesized[13] for a direct transition between Xe4 and Xe_p. Analysis of MD data showed that except for the DP−Xe4 ligand transition occurring in the nanoseconds time range, all of the other CO exchange rates are remarkably fast. This is well illustrated by considering the time dependence of the CO distribution among the xenon cavities, that is, P_{Xe1}/P_C, P_{Xe2}/P_C, P_{Xe3}/P_C, and P_{Xe4}/P_C, with P as the probability of a given CO site and $P_C = P_{Xe1} + P_{Xe2} + P_{Xe3} + P_{Xe4}$, as shown in Figure 2 (we omit in the figure the Xe3 fraction as it is negligible within the noise, indicating that this cavity is used to allow ligand transitions but it is a rather unstable CO site, at least for solvated Mb). From the figure, it is evident that for such a distribution, a full relaxation occurs within 1−2 ns, hence indicating that the mean lifetimes for the corresponding CO exchange rates are all within 400−500 ps.

The above scheme may then be simplified by grouping together Xe4, Xe3, and Xe_p as a single CO kinetic site C, whose internal distribution is in pre-equilibrium with respect to the other kinetic steps

$$\text{Mb} + \text{CO} \overset{k_e}{\leftarrow} \text{DP} \underset{k_{-1}}{\overset{k_1}{\rightleftarrows}} \text{C}$$

The last simple kinetic scheme (migration scheme), governed by three rate constants, is in marked contrast with the kinetic model obtained for crystallized Mb,[37] where the Xe4−Xe_p CO transition is the slow, irreversible within the time range investigated, kinetic process characterizing CO diffusion in the nanoseconds time range. Note also that in the present case, the Xe2 cavity is by far the principal CO site within C, different from the crystallized Mb where most of the ligand is accumulated in the Xe1 cavity. Moreover, in contrast to the crystal case where no CO escape was ever detected within the simulations,[37] our MD data for solvated Mb showed that a limited but significant CO fraction (about 0.2) escapes from the protein within the simulation time (15 ns), requiring the inclusion of such a step in the kinetic scheme. Interestingly, MD data also showed that only CO molecules located in the distal pocket were able to escape from the protein, indicating that other ligand exit sites, although possible, may be considered as secondary exit sites in wild-type Mb, in agreement with previous experimental and computational data.[51,52]

According to the migration scheme, we set the system of linear differential equations, parametrically dependent on the three microscopic rate constants, whose solution provides the complete (migration) relaxation kinetics, as described in detail in the Appendix. Solving the system of equations for different sets of the three rate constants, in a proper range, we were able to evaluate their values which best reproduce the kinetic trace provided by MD simulations. Such estimated microscopic rate constants ($k_1 = 2.02 \times 10^{-1}$ ns^{-1}, $k_{-1} = 1.07 \times 10^{-1}$ ns^{-1}, $k_e = 0.36 \times 10^{-1}$ ns^{-1} with relative standard errors of 5−10%) for CO intraprotein migration and escape determined the two eigenvalues ($\lambda_1 = -0.011$ ns^{-1}, $\lambda_2 = -0.333$ ns^{-1}) characterizing the complete ligand migration/escape kinetics (kinetic matrix eigenvalues; see the Appendix).

It is worth noting that the obtained kinetic matrix eigenvalues provide two relaxation processes of largely different time scales with $\lambda_2 \sim -(k_1 + k_{-1})$ corresponding to the DP−C ligand exchange relaxation rate and $\lambda_1 \sim -k_e\chi_{DP} = -k_e k_{-1}/(k_1 + k_{-1})$ providing the much slower ligand exit rate as given by a pre-equilibrium CO distribution inside of Mb; $\chi_{DP} = k_{-1}/(k_1 + k_{-1})$ is the equilibrium probability for a CO molecule within Mb to be located in the distal pocket, which is about 0.35 from our data.

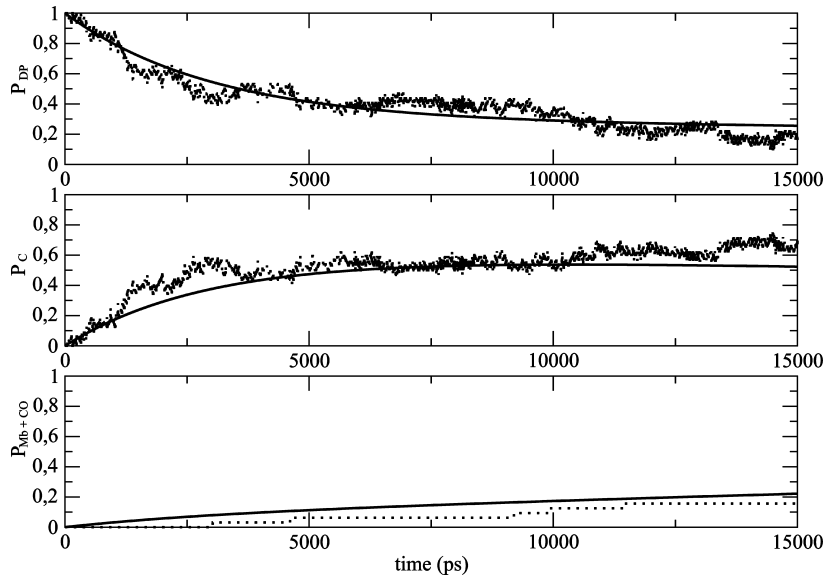

Figure 3. Kinetic trace of photolized CO occupancy (probability) for the three kinetic CO states considered in the migration scheme; MD data (dotted lines), kinetic model (solid lines).

Interestingly, the estimated mean lifetimes that we obtained for the DP to Xe4 transition, $1/k_1 = 5$ ns, and the ligand exit, $1/(k_e\chi_{DP}) = 80$ ns, are remarkably close to the corresponding values (4−5 and 113 ns, respectively) given in recent theoretical−computational works based on MD simulations.[51,52]

In Figure 3, we report the time course of CO occupancy, that is, the probability, for Mb ligand sites (DP, C) and free ligand state (Mb + CO), as obtained by MD simulations and evaluated by the theoretical kinetic model defined by the estimated eigenvalues. The accuracy of the model kinetics to reproduce MD data for all CO states demonstrates the reliability of the simple migration scheme used and the good convergence of the time-dependent occupancies provided by the 32 MD trajectories. These results clearly indicate that we may well describe the escape process in terms of a single (irreversible) kinetic step for the noncovalent complex Mb/CO = DP + C dissociation (i.e., pre-equilibrium CO distribution inside of Mb)

$$\mathrm{Mb/CO} \xrightarrow{\chi_{DP}k_e} \mathrm{Mb} + \mathrm{CO}$$
$$\dot{P}_{Mb/CO} = -\chi_{DP}k_e P_{Mb/CO} \quad (1)$$

where $P_{Mb/CO}$ is the probability of the noncovalent complex (we disregard as usual the rare case of more CO molecules inside of the protein).

Binding−Unbinding Kinetics. In our previous paper,[28] we obtained a quantitative description of the reaction free energy and related kinetics for the CO−heme bond formation−disruption in solvated Mb, as provided by PMM calculations[28,29,36] on the CO−heme covalent complex along the reaction coordinate (carbon−iron distance, i.e., the length of the carbon−iron connecting vector). However, in that paper, we investigated the reaction coordinate range (0.18−0.38 nm) corresponding only to the chemical bond formation−rupture, disregarding the unbound CO diffusion within the distal pocket. In this paper, combining the reaction free energy in the 0.12−0.38 nm reaction coordinate range as obtained by PMM[28] with the free-energy variation along the carbon−iron distance, beyond 0.38 nm, as provided by the unbound CO diffusion within the distal pocket as obtained by the present MD simulations (i.e., via the equilibrium distribution), we can evaluate the free-energy profile

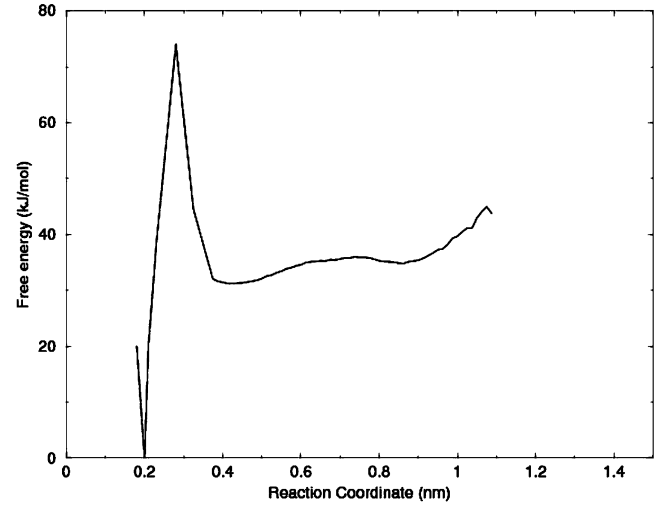

Figure 4. Free-energy profile (within distal pocket) along the CO−heme reaction coordinate (carbon−iron distance) as obtained by MD/PMM calculations.

for the complete binding−unbinding reaction step, as shown in Figure 4. Interestingly, the free-energy profile shows, besides the usual reaction minima close to the transition state, a third unexpected minimum, close to the DP−Xe4 border, probably due to the increased configurational freedom of the ligand once it passed the DP region occupied by the distal histidine side chain.

Hence, using the same kinetic model as that described in our previous papers,[28,36,53] on the basis of solving a Fokker−Planck equation for the diffusion process on the reaction free-energy surface and extracting from the solution the rate constants for the reactant−product conversion, we may express the kinetics for the binding−unbinding process via[28,36]

$$\mathrm{DP} \underset{K_{unb}}{\overset{K_{bi}}{\rightleftharpoons}} \mathrm{MbCO}$$
$$\dot{P}_{DP} = -K_{bin}P_{DP} + K_{unb}P_{MbCO}$$
$$\dot{P}_{MbCO} = K_{bin}P_{DP} - K_{unb}P_{MbCO} \quad (2)$$

with MbCO as the CO−heme bound state, P_{MbCO} the corresponding probability, and K_{unb} and K_{bin} the rate constants for

the unbinding and binding, respectively. Note that in the above binding−unbinding reaction scheme and coupled rate equations for P_{MbCO} and P_{DP}, following from the steady-state approximation for the transition-state (TS) probability as described in details in our previous paper,[28] the DP state (the unbound CO molecule within the distal pocket) corresponds to the 0.285−1.00 nm reaction coordinate range, while the bound CO state MbCO corresponds to the 0.125−0.275 nm reaction coordinate range (the TS is defined by the 0.275−0.285 nm range, and beyond 1 nm, the CO molecule enters into the Xe4 cavity). Note also that $K_{unb} = \kappa \exp(-\beta\Delta\mu^{\#}_{MbCO})$ and $K_{bin} = \kappa \exp(-\beta\Delta\mu^{\#}_{DP})$, where κ is a weakly temperature dependent factor, given by the microscopic rate constants for TS → MbCO and TS → DP transitions, providing the transition rate in the limit of ideal barrierless conditions, $\Delta\mu^{\#} = \Delta A^{\#}$ is the activation (Helmholtz) free energy as defined in our previous papers,[28,48] that is, variation of the standard chemical potential between the TS and the MbCO or DP state, and $1/\beta = k_B T$, with k_B as the Boltzmann constant and T the absolute temperature. The reaction free-energy profile shown in Figure 4 provides $\Delta\mu^{\#}_{MbCO} = 76$ kJ/mol and $\Delta\mu^{\#}_{DP} = 47$ kJ/mol (standard errors ∼ 1 kJ/mol), resulting in $K_{unb} = 4.5 \times 10^{-1}$ s^{-1} and $K_{bin} = 8.8 \times 10^{-2}$ μs^{-1}, corresponding to mean lifetimes of about 2 s and 11 μs, respectively, rather close to the corresponding values provided by the restricted (0.18−0.38 nm) reaction coordinate range used in our previous paper.[28] Note that the main effect of using the extended reaction coordinate range is the increase of the binding free-energy barrier, that is, the binding barrier as obtained by the restricted range is about 42 kJ/mol,[28] as a result of the increased ligand configurational freedom in the DP state.

Interestingly, both activation free energies are virtually temperature-independent, at least in the usual experimental temperature range, 278−300 K, as evidenced by low temperature tests (below 270 K, data not shown) and in line with results of previous papers.[53] Therefore, the activation free energy is virtually identical to the activation enthalpy, that is, the negligible activation entropy, and hence, $-\partial \ln K/\partial\beta \sim \Delta\mu^{\#}$.

Finally, the obtained binding−unbinding rate constants (K_{bin} and K_{unb}) providing kinetic relaxations in the microseconds and seconds range, respectively, clearly indicate that the CO distribution inside of Mb, occurring with a relaxation mean lifetime of about 3 ns, may be considered as virtually instantaneously equilibrated during the binding−unbinding kinetic step, similarly to CO escape, hence allowing the use of the noncovalent complex Mb/CO in the binding−unbinding reaction scheme and rate equations

$$\begin{gathered} \mathrm{Mb/CO} \underset{K_{unb}}{\overset{\chi_{DP}K_{bin}}{\rightleftharpoons}} \mathrm{MbCO} \\ \dot{P}_{Mb/CO} = -\chi_{DP}K_{bin}P_{Mb/CO} + K_{unb}P_{MbCO} \\ \dot{P}_{MbCO} = \chi_{DP}K_{bin}P_{Mb/CO} - K_{unb}P_{MbCO} \end{gathered} \tag{3}$$

Complete Process: CO Geminate Binding, Escape, and Thermal Dissociation. In the previous two subsections, we showed that both the CO binding and escape kinetic steps can be considered as occurring with a pre-equilibrium CO distribution inside of Mb, hence allowing the use of the noncovalent complex Mb/CO in the kinetic schemes. With such results, we are able to describe the whole kinetic process, involving geminate binding and escape, by combining the schemes and rate equations (eqs 1−3) obtained in the previous subsections

$$\begin{gathered} \mathrm{Mb} + \mathrm{CO} \overset{\chi_{DP}k_e}{\longleftarrow} \mathrm{Mb/CO} \underset{K_{unb}}{\overset{\chi_{DP}K_{bin}}{\rightleftharpoons}} \mathrm{MbCO} \\ \dot{P}_{Mb/CO} = -\chi_{DP}(k_e + K_{bin})P_{Mb/CO} + K_{unb}P_{MbCO} \\ \dot{P}_{MbCO} = \chi_{DP}K_{bin}P_{Mb/CO} - K_{unb}P_{MbCO} \end{gathered} \tag{4}$$

The last scheme and rate equations, equivalent to the kinetic model assumed by Henry et al.[14] to describe room-temperature (295 K) experimental data except for the ligand/protein association neglected in our model, may be utilized to obtain the kinetics for the two usual conditions considered, the CO−heme thermal dissociation characterized by the $P_{MbCO}(0) = 1$ boundary condition and after photolysis relaxation characterized by the $P_{Mb/CO}(0) = 1$ boundary condition.

For the former case, we may assume, as usual, the steady-state condition $\dot{P}_{Mb/CO} \cong 0$, providing the equations[14,21,54]

$$\begin{gathered} \dot{P}_{MbCO} \cong -K_{off}P_{MbCO} \\ K_{off} = (1 - \phi)K_{unb} \\ \phi = \frac{K_{bin}}{k_e + K_{bin}} \end{gathered} \tag{5}$$

with solution

$$P_{MbCO}(t) \cong \exp(-K_{off}t) \tag{6}$$

In the latter case, we can fully disregard the unbinding process as $K_{unb}/K_{bin} \cong 0$, hence obtaining

$$\begin{gathered} \dot{P}_{Mb/CO} \cong -K_{gem}P_{Mb/CO} \\ \dot{P}_{MbCO} \cong \chi_{DP}K_{bin}P_{Mb/CO} \end{gathered} \tag{7}$$

$$K_{gem} = \chi_{DP}(k_e + K_{bin}) \tag{8}$$

providing the familiar geminate relaxation equations[14,18,21]

$$\begin{gathered} P_{Mb/CO}(t) \cong \exp(-K_{gem}t) \\ P_{MbCO}(t) \cong \phi[1 - \exp(-K_{gem}t)] \end{gathered} \tag{9}$$

The above kinetic equations derived from unbiased theoretical−computational data clearly show that the simple kinetic scheme proposed by Henry et al. to describe room-temperature experimental data[14,18,20−22,54] is consistent with the kinetic mechanism and relaxation behavior provided by the model system used in our calculations. It must be noted that the rate constants defining the complete process as provided by our MD/PMM model, within the noise, match well the corresponding values as obtained from experimental data[14,21,55−57] (see Table 1), suggesting that the quantum mechanical (PMM) calculations and MD atomistic model used reproduce the essential physics of the system considered (the differences between the rate constants provided by our theoretical−computational model and the corresponding values as obtained by experimental data correspond to only a few kJ/mol in the activation

TABLE 1: Comparison of Kinetic Properties for Mb/CO Geminate Binding, Escape, and Thermal Dissociation as Obtained by MD/PMM Calculations (this work) and Experimentally Derived at 293[21] and 295 K[14]

	MD/PMM 293 K	exp. data 293 K	exp. data 295 K
$1/K_{unb}$ (s)	2.2	50.0	55.5
$1/K_{off}$ (s)	2.2	52.6	55.8
$1/(\chi_{DP}K_{bin})$ (μs)	32.5	5.0	4.3
$1/(\chi_{DP}k_e)$ (ns)	80	200	192
ϕ	0.25%	3.9%	4.3%
$1/K_{gem}$ (ns)	80	196	182

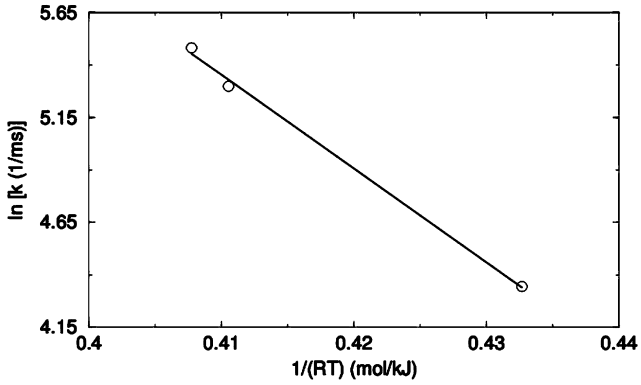

Figure 5. Arrhenius plot as obtained by experimental CO−heme binding rate constants at 278,[18] 293,[21] and 295 K;[14] experimental data (circles), linear regression (solid line).

free energies, either within the noise or possibly due to small entropic terms neglected in our calculations[28,36] and/or slight inaccuracies of ab initio quantum calculations and MD force field). By using experimental kinetic data at 278,[18] 293,[21] and 295 K[14] and considering χ_{DP} as essentially constant in the temperature range of interest, we evaluated (via the Arrhenius plot in Figure 5) the activation enthalpy for the binding step DP → MbCO resulting in a value of about 45 kJ/mol, remarkably close to the activation enthalpy that we obtained (47 kJ/mol, see previous subsection) and in reasonable agreement with a previous experimental evaluation (33−34 kJ/mol) as obtained by room-temperature data.[22] Such values are significantly higher than the corresponding activation enthalpy (10−20 kJ/mol) estimated by extrapolating low-temperature data and/or using high-viscosity conditions,[15,16] suggesting a possible relevant Mb conformational/statistical mechanical reorganization due to temperature and viscosity, essentially driven by entropic effects. Interestingly, the pre-exponential constant as obtained by the Arrhenius plot in Figure 5 (18.6 ps^{-1}) almost exactly matches the corresponding value provided by our MD/PMM model ($\chi_{DP}\kappa = 7.4\ ps^{-1}$), further showing the robustness of the theoretical approach employed.

Conclusions

In this paper, the combined use of MD simulations and quantum mechanical calculations (PMM) allowed the construction of a detailed (unbiased) kinetic model for room-temperature CO binding, migration, and escape in solvated wild-type Mb, resulting in a simple exponential CO geminate binding and escape relaxation which is fully consistent with the phenomenological model[14] widely utilized to describe Mb/CO room-temperature experimental data.[14−16,18,20−22] Our theoretical−computational study provided no evidence (at least within the time range investigated) for slow Mb conformational transitions and multiple CO migration relaxations possibly involved in geminate binding and escape reactions. Interestingly, our calculations, providing a good reproduction of experimental rate constants, furnished an estimate of the CO−heme binding activation enthalpy, which is significantly higher than values[15,16] obtained by extrapolating low-temperature data and/or using high-viscosity conditions but remarkably close to the estimate that we obtained utilizing experimental data at 278,[18] 293,[21] and 295 K[14] and in reasonable agreement with a previous experimental evaluation based on room-temperature data.[22] Such a discrepancy might suggest that a relevant conformational transition and/or statistical mechanical reorganization in the Mb/CO system may occur as the temperature increases, leading to a significantly different binding energy barrier at room temperature.

Moreover, our results show that CO migration in solvated Mb is characterized by picoseconds relaxations for CO transitions among Mb cavities, with the exception of the nanoseconds-range DP−Xe4 CO exchange, which is hence the rate-limiting step of CO (intra-Mb) migration kinetics. This is in marked contrast with the kinetic model that we obtained from MD data of crystallized Mb,[37] indicating that kinetic schemes and properties as obtained in a given Mb/CO condition (defined by temperature, aggregation state, mutations, etc.) cannot simply be used and/or extrapolated for different systems' conditions.

Finally, the present work, to our knowledge providing for the first time a quantitative model for the complete Mb/CO reaction process based on atomistic simulations, rigorous quantum calculations, and proper statistical mechanical treatment, clearly shows that advanced, but nowadays computationally feasible, theoretical modeling may really provide an accurate description of complex biomolecular processes, opening the way to deeper and more effective collaborations between theoreticians and experimentalists.

Acknowledgment. This work was supported by the Italian PRIN Project N. 20074TJ3ZB_002 "Structure and dynamics of redox proteins: theoretical and computational approach" founded by MIUR. We also acknowledge the University of Rome "La Sapienza" for financial support with the project Project N. C26A09JKNF and CASPUR (Consorzio interuniversitario per le Applicazioni di Supercalcolo Per Università e Ricerca) for the use of its computational facilities.

Appendix

According to the migration kinetic scheme (see Results section), we may set the system of differential rate equations providing the kinetics (probability time dependence) of the two relevant CO states within Mb (DP and C; see Results section)

$$\begin{cases} \dot{P}_{DP} = -(k_1 + k_e)P_{DP} + k_{-1}P_C \\ \dot{P}_C = k_1 P_{DP} - k_{-1}P_C \end{cases} \quad \text{(A1)}$$

with P_{DP} and P_C as the corresponding probabilities, which may be expressed by the more compact matrix equation $\dot{\mathbf{P}} = \tilde{\mathbf{K}}\mathbf{P}$, where

$$\tilde{\mathbf{K}} \equiv \begin{bmatrix} -(k_1 + k_e) & k_{-1} \\ k_1 & -k_{-1} \end{bmatrix} \qquad \mathbf{P} \equiv \begin{bmatrix} P_{DP} \\ P_C \end{bmatrix} \qquad \dot{\mathbf{P}} \equiv \begin{bmatrix} \dot{P}_{DP} \\ \dot{P}_C \end{bmatrix}$$

Introducing the linear transformation $\tilde{\mathbf{T}} \equiv [\boldsymbol{\eta}_1\ \boldsymbol{\eta}_2]$, which diagonalizes the kinetic matrix $\tilde{\mathbf{K}}$, defined by the eigenvectors of $\tilde{\mathbf{K}}$, we may readily obtain

$$\mathbf{P}(t) = \tilde{\mathbf{T}} \begin{bmatrix} e^{\lambda_1 t} & 0 \\ 0 & e^{\lambda_2 t} \end{bmatrix} \tilde{\mathbf{T}}^{-1}\mathbf{P}(0) \quad \text{(A2)}$$

where λ_1 and λ_2 are the kinetic matrix eigenvalues. Finally, from eq A2, we can obtain the probability time dependence for each kinetic state in the migration scheme, including the one for the free ligand state via the relation $P_{Mb+CO} = 1 - P_{Mb/CO} - P_{MbCO}$.

Supporting Information Available: Figure S1 showing the time evolution of the transition numbers for the forward and backward ligand exchange between cavities is provided. This

material is available free of charge via the Internet at http://pubs.acs.org.

References and Notes

(1) Austin, R. H.; Beeson, K. W.; Eisenstein, L.; Frauenfelder, H.; Gunsalus, I. C. Dynamics of ligand binding to myoglobin. *Biochemistry* **1975**, *14*, 5355–5373.

(2) Scott, E. E.; Gibson, Q. H.; Olson, J. S. Mapping the pathways for O_2 entry into and exit from myoglobin. *J. Biol. Chem.* **2001**, *276*, 5177–5188.

(3) Tilton, R. F., Jr.; Kuntz, I. D., Jr.; Petsko, G. A. Cavities in proteins: structure of a metmyoglobin−xenon complex solved to 1.9 A. *Biochemistry* **1984**, *23*, 2849–2857.

(4) Srajer, V.; Teng, T.; Ursby, T.; Pradervand, C.; Ren, Z.; Adachi, S.; Schildkamp, W.; Bourgeois, D.; Wulff, M.; Moffat, K. Photolysis of the carbon monoxide complex of myoglobin: nanosecond time-resolved crystallography. *Science* **1996**, *274*, 1726–1729.

(5) Srajer, V.; Ren, Z.; Teng, T. Y.; Schmidt, M.; Ursby, T.; Bourgeois, D.; Pradervand, C.; Schildkamp, W.; Wulff, M.; Moffat, K. Protein conformational relaxation and ligand migration in myoglobin: a nanosecond to millisecond molecular movie from time-resolved Laue X-ray diffraction. *Biochemistry* **2001**, *40*, 13802–13815.

(6) Bourgeois, D.; Vallone, B.; Arcovito, A.; Sciara, G.; Schotte, F.; Anfinrud, P. A.; Brunori, M. Extended subnanosecond structural dynamics of myoglobin revealed by Laue crystallography. *Proc. Natl. Acad. Sci. U.S.A.* **2006**, *103*, 4924–4929.

(7) Bourgeois, D.; Vallone, B.; Schotte, F.; Arcovito, A.; Miele, A. E.; Sciara, G.; Wulff, M.; Anfinrud, P.; Brunori, M. Complex landscape of protein structural dynamics unveiled by nanosecond Laue crystallography. *Proc. Natl. Acad. Sci. U.S.A.* **2003**, *100*, 8704–8709.

(8) Schmidt, M.; Nienhaus, K.; Pahl, R.; Krasselt, A.; Anderson, S.; Parak, F.; Nienhaus, G. U.; Srajer, V. Ligand migration pathway and protein dynamics in myoglobin: A time-resolved crystallographic study on L29W MbCO. *Proc. Natl. Acad. Sci. U.S.A.* **2005**, *102*, 11704–11709.

(9) Schotte, F.; Lim, M.; Jackson, T. A.; Smirnov, A. V.; Soman, J.; Olson, J. S.; Phillips, G. N., Jr.; Wulff, M.; Anfinrud, P. A. Watching a protein as it functions with 150-ps time-resolved X-ray crystallography. *Science* **2003**, *300*, 1944–1947.

(10) Schotte, F.; Soman, J.; Olson, J. S.; Wulff, M.; Anfinrud, P. A. Picosecond time-resolved X-ray crystallography: probing protein function in real time. *J. Struct. Biol.* **2004**, *147*, 235–246.

(11) Teng, T. Y.; Srajer, V.; Moffat, K. Photolysis-induced structural changes in single crystals of carbonmonoxy myoglobin at 40 K. *Nat. Struct. Biol.* **1994**, *1*, 701–705.

(12) Teng, T. Y.; Srajer, V.; Moffat, K. Initial trajectory of carbon monoxide after photodissociation from myoglobin at cryogenic temperatures. *Biochemistry* **1997**, *36*, 12087–12100.

(13) Tomita, A.; Sato, T.; Ichiyanagy, K.; Nozawa, S.; Ichikawa, H.; Chollet, M.; Kawai, F.; Park, S. Y.; Tsuduki, T.; Yamato, T.; Koshihara, S. Y.; Adachi, S. I. Visualizing breathing motion of internal cavities in concrt with ligand migration in myoglobin. *Proc. Natl. Acad. Sci. U.S.A.* **2009**, *106*, 2612–2616.

(14) Henry, E. R.; Sommer, J. H.; Hofrichter, J.; Eaton, W. A. Geminate recombination of carbon monoxide to myoglobin. *J. Mol. Biol.* **1983**, *166*, 443–451.

(15) Austin, R. H.; Beeson, K. W.; Frauenfelder, H.; Gunsalus, I. C. Dynamics of ligand binding. *Biochemistry* **1975**, *14*, 5355–5373.

(16) Steinbach, P. J.; Ansari, A.; Berendzen, J.; Braunstein, D.; Chu, K.; Cowen, B. R.; Ehrenstein, D.; Frauenfelder, H.; Johnson, J. B.; Lamb, D. C.; Luck, S.; Mourant, J. R.; Nienhaus, G. U.; Ormos, P.; Philipp, R.; Xie, A.; Young, R. D. Ligand binding to heme proteins: connection between dynamics and function. *Biochemistry* **1991**, *30*, 3988–4001.

(17) Tian, W. D.; Sage, J. T.; Champion, P. M. Investigation of ligand association and dissociation rates in the "open" and "closed" states of myoglobin. *J. Mol. Biol.* **1993**, *233*, 155–166.

(18) Sugimoto, T.; Unno, M.; Shiro, Y.; Dou, Y.; Ikrda-Saito, M. Myoglobin mutants giving the largest geminate yield in CO rebinding in the nanosecond time domain. *Biophys. J.* **1998**, *75*, 2188–2194.

(19) Dadusc, G.; Ogilvie, J. P.; Schulenberg, P.; Marvet, U.; Dwayne Miller, R. J. Diffractive optics-based heterodyne-detected four-wave mixing signals of protein motion: from "protein quakes" to ligand escape for myoglobin. *Proc. Natl. Acad. Sci. U.S.A.* **2001**, *98*, 6110–6115.

(20) Carver, T. E.; Rohlfs, R. J.; Olson, J. S.; Gibbson, Q. H.; Blackmore, R. S.; Spinger, B. A.; Sligar, S. G. Analysis of the kinetic barrier for ligand binding to sperm whale myoglobin using site-directed mutagenesis and laser photolysis techniques. *J. Biol. Chem.* **1990**, *265*, 2007–20020.

(21) Dantsker, D.; Roche, C.; Samuni, U.; Blauin, G.; Olson, J. S.; Friedman, J. M. The position 68(E11) side chain in myoglobin regulates ligand capture, bond formation with heme iron, and internal movement into xenon cavities. *J. Biol. Chem.* **2005**, *280*, 38740–38755.

(22) Goldbeck, R. A.; Bhaskaran, S.; Ortega, C.; Mendoza, J. L.; Olson, J. S.; Soman, J.; Kliger, D. S.; Esquerra, R. M. Water and ligand entry in myoglobin: asswssing the speed and extent of heme pocket hydration after CO photodissociation. *Proc. Natl. Acad. Sci. U.S.A.* **2006**, *103*, 1254–1259.

(23) Ansari, A.; Jones, C. M.; Henry, E. R.; Hofrichter, J.; Eaton, W. A. Conformational relaxation and ligand binding in myoglobin. *Biochemistry.* **1994**, *33*, 5128–5145.

(24) Harvey, J. N. DFT computation of the intrinsic barrier to CO geminate recombination with heme compounds. *J. Am. Chem. Soc.* **2000**, *122*, 12401–12402.

(25) Franzen, S. Spin-dependent mechanism for diatomic ligand binding to heme. *Proc. Natl. Acad. Sci. U.S.A.* **2002**, *99*, 16754–16759.

(26) Starovoitov, V. S.; Dzhagarov, B. M. A diffusion-based approach to geminate recombination of heme proteins with small ligands. *Chem. Phys.* **2003**, *292*, 1–10.

(27) Banushkina, P.; Meuwly, M. Free-energy barriers in MbCO rebinding. *J. Phys. Chem. B* **2005**, *109*, 16911–16917.

(28) Amadei, A.; D'Abramo, M.; Daidone, I.; D'Alessandro, M.; Di Nola, A.; Aschi, M. Statistical mechanical modelling of chemical reactions in complex systems: the kinetics of the haem carbon monoxide binding-unbinding reaction in myoglobin. *Theor. Chem. Acc.* **2007**, *117*, 637–647.

(29) Amadei, A.; D'Alessandro, M.; Aschi, M. Statistical mechanical modeling of chemical reactions in complex systems: the reaction free energy surface. *J. Phys. Chem. B* **2004**, *108*, 16250–16254.

(30) Aschi, M.; Spezia, R.; Di Nola, A.; Amadei, A. A first principles method to model perturbed electronic wavefunctions: the effect of an external electric field. *Chem. Phys. Lett.* **2001**, *344*, 347–380.

(31) Amadei, A.; Marinelli, F.; D'Abramo, M.; D'Alessandro, M.; Anselmi, M.; Di Nola, A.; Aschi, M. Theoretical modeling of vibro-electronic quantum states in complex molecular systems: solvated carbon monoxide a test case. *J. Chem. Phys.* **2005**, *122*, 124506.

(32) Amadei, A.; D'Alessandro, M.; D'Abramo, M.; Aschi, M. Theoretical characterization of electronic states in interacting chemical systems. *J. Chem. Phys.* **2009**, *130*, 084109.

(33) D'Abramo, M.; Di Nola, A.; Aschi, M.; Amadei, A. Theoretical characterization of temperature and density dependence of liquid water electronic excitation energy: comparison with recent experimental data. *J. Chem. Phys.* **2008**, *128*, 021103.

(34) Anselmi, M.; Aschi, M.; Di Nola, A.; Amadei, A. Theoretical characterization of carbon monoxide vibrational spectrum in sperm whale myoglobin. *Biophys. J.* **2007**, *92*, 3442–3447.

(35) Amadei, A.; D'Alessandro, M.; Paci, M.; Di Nola, A.; Aschi, M. On the effect of a point mutation on the reactivity of CuZn superoxide dismutase: a theoretical study. *J. Phys. Chem. B* **2006**, *110*, 7538–7544.

(36) Amadei, A.; Aschi, M.; Di Nola, A. Statistical mechanical modeling of chemical reactions in condensed systems. In *Solvation effects on molecules and biomolecules*; Canuto S., Ed.; Challenges and advances in computational chemistry and physics; Springer: New York, 2008; Vol. 6, pp 191−213.

(37) Anselmi, M.; Di Nola, A.; Amadei, A. The kinetics of carbon monoxide migration in crystallized myoglobin as revealed by molecular dynamics simulations. *Biophys. J.* **2008**, *94*, 4277–4281.

(38) Berendsen, H. J. C.; Postma, J. P. M.; van Gunsteren, W. F.; Hermans. J. Interaction models for water in relation to protein hydration. In *Intermolecular Forces*; Pullman, B., Ed.; D. Reidel Publishing Company: Dordrecht, The Netherlands, 1981; pp 331−342.

(39) Berendsen, H. J. C.; van der Spoel, D.; van Drunen., R. GROMACS: A message-passing parallel molecular dynamics implementation. *Comput. Phys. Commun.* **1995**, *91*, 43–56.

(40) van Gunsteren, W. F.; Billeter, S.; Eising, A.; Hunenberger, P.; Kruger, P.; Mark, A. E.; Scott, W.; Tironi, I. *Biomolecular Simulations: The GROMOS96 Manual and User Guide*; BIOMOS bv: Zurich, Groningen, 1996.

(41) Straub, J. E.; Karplus, M. Molecular dynamics study of the photodissociation of carbon monoxide from myoglobin: ligand dynamics in the first 10 ps. *Chem. Phys.* **1991**, *158*, 221–248.

(42) De Angelis, F.; Jarzecki, A. A.; Car, R.; Spiro, T. G. Quantum chemical evaluation of protein control over heme ligation: CO/O_2 discrimination in myoglobin. *J. Phys. Chem. B* **2005**, *109*, 3065–3070.

(43) Merchant, K. A.; Thompson, D. E.; Xu, Q.-H.; Williams, R. B.; Loring, R. F.; Fayer, M. D. Myoglobin−CO conformational substate dynamics: 2D vibrational echoes and MD simulations. *Biophys. J.* **2002**, *82*, 3277–3288.

(44) Nienhaus, K.; Olson, J. S.; Franzen, S.; Nienhaus, G. U. The origin of stark splitting in the initial photoproduct state of MbCO. *J. Am. Chem. Soc.* **2005**, *127*, 40–41.

(45) Nutt, D. R.; Meuwly, M. Theoretical investigation on infrared spectra and pocket dynamics of photodissociated carbonmonoxy myoglobin. *Biophys. J.* **2003**, *85*, 3612–3623.

(46) Evans, D. J.; Morriss. G. P. *Statistical Mechanics of Nonequilibrium Liquids*; Academic: London, 1990.

(47) Hess, B.; Bekker, H.; Berendsen, H. J. C.; Fraaije, J. G. E. M. LINCS: a linear constraint solver for molecular simulations. *J. Comput. Chem.* **1997**, *18*, 1463–1472.

(48) Essmann, U.; Perera, L.; Berkowitz, M. L.; Darden, T.; Lee, H.; Pedersen., L. G. A smooth particle mesh Ewald method. *J. Chem. Phys.* **1995**, *103*, 8577–8593.

(49) Bossa, C.; Anselmi, M.; Roccatano, D.; Amadei, A.; Vallone, B.; Brunori, M.; Di Nola, A. Extended molecular dynamics simulation of the carbon monoxide migration in sperm whale myoglobin. *Biophys. J.* **2004**, *86*, 3855–3862.

(50) Bossa, C.; Amadei, A.; Daidone, I.; Anselmi, M.; Vallone, B.; Brunori, M.; Di Nola, A. Molecular dynamics simulation of sperm whale myoglobin: effects of mutations and trapped CO on the structure and dynamics of cavities. *Biophys. J.* **2005**, *89*, 465–474.

(51) Anselmi, M.; Aschi, M.; Di Nola, A.; Amadei, A. Theoretical characterization of carbon monoxide vibrational spectrum in sperm whale myoglobin distal pocket. *Biophys. J.* **2007**, *92*, 3442–3447.

(52) Ruscio, J. Z.; Kumar, D.; Shukla, M.; Prisant, M. G.; Murali, T. M.; Onufriev, A. V. Atomic level computational identification of ligand migration pathways between solvent and binding site in myoglobin. *Proc. Natl. Acad. Sci. U.S.A.* **2008**, *105*, 9204–9209.

(53) Aschi, M.; D'Abramo, M.; Ramondo, F.; Daidone, I.; D'Alessandro, M.; Di Nola, A.; Amadei, A. Theoretical modeling of chemical reactions in complex environments: the intramolecular proton transfeer in aqueous malonaldehyde. *J. Phys. Org. Chem.* **2006**, *19*, 518–530.

(54) Moffet, D. A.; Case, M. A.; House, J. C.; Vogel, K.; Wiliams, R. D.; Spiro, T. G.; McLendon, G. L.; Hecht, M. H. Carbon monoxide binding by de novo heme proteins derived from designed combinatorial libraries. *J. Am. Chem. Soc.* **2001**, *123*, 2109–2115.

(55) Olson, J. S.; Phillips, G. N. Kinetic pathways and barriers for ligand binding to myoglobin. *J. Biol. Chem.* **1996**, *271*, 17593–17596.

(56) Lim, M.; Jackson, T. A.; Anfirud., P. A. Binding of CO to myoglobin from a heme pocket docking site to form nearly linear Fe−CO. *Science* **1995**, *269*, 962–966.

(57) Lim, M.; Jackson, T. A.; Anfirud., P. A. Mid-infrared vibrational spectrum of CO after photodissociation from heme: evidence for a ligand docking site in the heme pocket of hemoglobin and myoglobin. *J. Chem. Phys.* **1995**, *102*, 4355–4366.

JP903165P